



1 Time evolution of observed July–September sea surface 2 temperature–Sahel climate teleconnection with removed 3 quasi-global effect (1900–2008)

4 Bernard Fontaine,¹ Marco Gaetani,² Albin Ullmann,¹ and Pascal Roucou¹

5 Received 30 July 2010; revised 10 December 2010; accepted 29 December 2010; published XX Month 2011.

6 [1] Using sea surface temperature (SST), precipitation, and atmospheric information, this
7 statistical study revisits the questions of the July–September SST–Sahel teleconnection
8 variability after removing impact of quasi-global SSTs over the period 1900–2008. The
9 eastern Mediterranean and the Indian Ocean dominate the relationship, both in terms of
10 intensity and time stability, with significant values in 52% and 47% of years, respectively.
11 More than two thirds of the rainy seasons classified as dry (wet) and 16 out of 18 (12 out
12 of 15) of those classified as very dry (very wet) are concomitant of negative (positive)
13 differences between the Mediterranean and the Indian Ocean. Correlations with the
14 tropical Atlantic, the Niño area, and the western Pacific region are generally lower and less
15 robust, although, in some periods, they can be high with the southern tropical Atlantic.
16 Teleconnection observed with continental precipitation and the 950 hPa moisture flux field
17 confirmed these results. Positive SST differences between the eastern Mediterranean and
18 the Indian Ocean are synchronous of in-phase rainfall excess over the whole Sudan–
19 Sahel due to a strengthening of the convergence between the northeasterly moisture
20 transport from the eastern Mediterranean and the monsoon southwesterly moisture
21 transport from the eastern equatorial Atlantic. This is associated with changes in the
22 atmospheric circulation along the meridional and zonal planes, mainly (1) a subsidence
23 departure from midlevels above 10°N–18°N associated with air ascents above the Saharan
24 thermal lows, (2) upward anomalies on the western and eastern Sahel reinforcing the
25 atmospheric ascents in upper levels, (3) a low-level subsidence anomaly by 30°E–40°E in
26 agreement with the Indian cooling weakening the normal uplifts, and (4) a reinforcement
27 of the tropical easterly jet over 0°–20°E.

28 **Citation:** Fontaine, B., M. Gaetani, A. Ullmann, and P. Roucou (2011), Time evolution of observed July–September sea surface
29 temperature–Sahel climate teleconnection with removed quasi-global effect (1900–2008), *J. Geophys. Res.*, 116, XXXXXX,
30 doi:10.1029/2010JD014843.

31 1. Introduction

32 [2] The objective of this study is to revisit the question of
33 the summertime SST–Sahel teleconnection variability along
34 the twentieth century using both several gridded data sets for
35 describing time evolution of the basic fields (SST, precipi-
36 tation, atmospheric circulation) and selected key SST
37 indexes and atmospheric descriptors representative of the
38 West African monsoon.

39 [3] The question is to what extent have quasi-global SST
40 and basin-scale variations contributed to the observed
41 changes in the teleconnection, i.e., to the long-term evolu-
42 tion of correlation patterns defined at an interannual time
43 step. The purpose is therefore different from previous

studies which often have documented this relationship 44
without removing the global warming effect. In this work 45
we have chosen to separate thermal evolutions observed in 46
the different oceanic basins, including the Mediterranean, 47
from the global-scale SST (GSST) influence, regardless of 48
its natural or anthropogenic origin. Removing the GSST- 49
related influence has a significant effect on long-term SST 50
evolution in the oceanic basins and allows us to separate 51
better basin-scale variability from longer-term evolutions 52
and, therefore, to quantify suitably their relative statistical 53
impacts on Sahelian rainfall. In addition, the investigation of 54
the Mediterranean role in the variability of the Sahelian 55
precipitation on a multidecadal time scale represents an 56
outstanding effort in filling this gap in the knowledge of the 57
West African monsoon teleconnections. Using linear cor- 58
relations, multiple regressions, composite methods and 59
cluster analyses we discuss the results in terms of statistical 60
significance and time stability over various periods ranging 61
between 1900 and 2008. Furthermore, we conclude by a 62
short analysis of the atmospheric circulation in terms of 63

¹Centre de Recherches de Climatologie, CNRS/Université de Bourgogne, Dijon, France.

²Istituto di Biometeorologia, IBIMET-CNR, Rome, Italy.

64 moisture transport, and large-scale divergent meridional and
65 zonal circulation, in order to highlight the association with
66 the SST time evolution.

67 2. Review of the Literature

68 [4] The relationship between sea surface temperature
69 (SST) fields and summer Sahel rainfall has been studied for
70 a long time, emphasizing the potential role of tropical
71 Oceanic basins [e.g., *Hastenrath and Lamb*, 1977; *Lamb*,
72 1978; *Lough*, 1986; *Folland et al.*, 1986; *Palmer*, 1986;
73 *Nicholson and Nyenzi*, 1990; *Ward et al.*, 1990]. Overall
74 these authors showed that warmer (colder) waters southward
75 to the equator—relative to that northward—were often asso-
76 ciated with Sahelian drier (wetter) conditions over the Sahel.
77 In particular, *Folland et al.* [1986] have been the first au-
78 thors who linked Sahelian rainfall long-term variability to
79 the differential SST warming between the hemispheres
80 through the latitudinal location of the ITCZ over the
81 Atlantic. This statistical teleconnection, observed both at the
82 interannual and decadal scales, is in good agreement with
83 model results and hence can be interpreted in terms of
84 Oceanic forcing on the tropical circulation. In the Atlantic,
85 for example, *Hastenrath and Polzin* [2011] show that
86 warmer (cooler) surface waters over the tropical North
87 Atlantic accompanied by lower (higher) surface pressure
88 enhance (decrease) the cross-equatorial winds from the
89 Southern Hemisphere and hence precipitation in the Sahel.
90 In the ARPEGE AGCM, the simulated drought is associated
91 with a southward shift of the continental rainbelt over cen-
92 tral and eastern Sahel, linked to an interhemispheric SST
93 mode, the southern hemisphere oceans warming faster than
94 the northern ones after 1970 [*Caminade and Terray*, 2010].
95 Other model experiments [*Losada et al.*, 2009] indicate that
96 warmer SST anomalies in the equatorial Atlantic lead to a
97 decrease of the local surface temperature gradient, weak-
98 ening the West African monsoon flow and the surface
99 convergence over the Sahel. *Ward* [1998] and *Joly and*
100 *Voldoire* [2010] state that the main oceanic sources of sea-
101 sonal rainfall predictability over West Africa are SST
102 anomalies in the equatorial Pacific, the equatorial Atlantic
103 and the Mediterranean.

104 [5] Possible causes and impacts of SST variability at
105 longer term have been also pointed out. Thus *Delworth et al.*
106 [1993] described thermal impacts of the North Atlantic
107 thermohaline overturning circulation at multidecadal scales:
108 the resulting SST pattern is known as the Atlantic Multi-
109 decadal Oscillation (AMO) [*Goldenberg et al.*, 2001; *Zhang*
110 *and Delworth*, 2006]. *Bader and Latif* [2003] identified the
111 warming of the Indian Ocean—partly due to anthropogenic
112 greenhouse gases [*Stott et al.*, 2000]—as a potential source of
113 Sahelian drying. They suggested that warming trends in the
114 Indian Ocean played a crucial role for the drying trend over
115 the West Sahel from the 1950s to 1990s, while the tropical
116 Pacific's influence is predominantly over the East Sahel and
117 the tropical Atlantic impacts rainfall only along the Guinea
118 Coast. More recently, focusing on the very dry year 1983,
119 *Bader and Latif* [2011], showed that the Indian Ocean sig-
120 nificantly affects interannual rainfall variability over the
121 west Sahel. In particular, they provide evidence that the
122 remanence from the strong 1982/1983 El Niño event in this

ocean was the main forcing for the drought observed in 123
1983 over the Sahel. 124

[6] Studying the ENSO-Sahel relationship, *Janicot et al.* 125
[2001] proposed that the existence of periods of weak or 126
strong linkage could result from an interaction with the 127
global decadal-scale SST variability, which is able to 128
enhance the impact of the warm ENSO phases after 1980, 129
through an increase in the fill-in of the monsoon trough and 130
a moisture advection deficit over West Africa. In addition, 131
Giannini et al. [2003] related the warming of the low-lati- 132
tude waters around Africa to the recent negative precipita- 133
tion trend in the Sahel, hypothesizing that the favored deep 134
convection over the ocean could weaken the monsoonal 135
convergence over the continent. More generally the drying 136
trend observed in the Sahel from the 1950s to the mid 1980s 137
coincides with marked decadal shifts like those in the 138
Atlantic Multidecadal Oscillation, the Pacific Decadal 139
Oscillation, the low-frequency component of the Atlantic 140
Niño and the global temperature [*Rodriguez de Fonseca* 141
et al., 2011]. 142

[7] The linkage between the local forcing and the remote 143
SST signals implied in the Sahel/SST teleconnection has 144
been also discussed. For example, *Rowell et al.* [1995] 145
showed that SSTA linked to the Niño/Nina variability im- 146
pacts indirectly on July–August–September Sahelian rainfall 147
via atmospheric teleconnection generating SST anomalies in 148
the Atlantic. *Rodriguez-Fonseca et al.* [2009] presented 149
observational evidence of a change in the Atlantic–Pacific 150
Niños connection since the late 1960s. The role of the 151
eastern Mediterranean basin in the determination of the 152
interannual variability of the monsoonal precipitation has 153
been highlighted by *Rowell* [2003] and *Fontaine et al.* 154
[2009]: warm SST anomalies positively affect the Sahelian 155
precipitation in July–August–September in reinforcing the 156
moisture transport from the Mediterranean across the Sahara 157
and hence the moisture flux convergence over the Sahel. 158

[8] Thus the SST forcing can be considered as the domi- 159
nant driver of West African rainfall variability. Conversely it 160
is not the unique factor impacting rainfall in this monsoon 161
region for at least three reasons: (1) atmospheric internal 162
variability contributes strongly to driving the simulated 163
precipitation variability over the Sahel at decadal to multi- 164
decadal time scales [*Caminade and Terray*, 2010], (2) land 165
surface vegetation processes and dust feedbacks may amplify 166
rainfall anomalies [*Biasutti et al.*, 2008], and (3) global 167
warming impacts both multidecadal SST variability and 168
monsoon circulation [*Paeth and Hense*, 2004]. 169

[9] Indeed West Africa is sensitive to water vapor and 170
lapse rate, vegetation, surface albedo, clouds and also 171
aerosols. For example, aerosol feedbacks may act to amplify 172
the ocean-forced component of monsoon circulation: the 173
direct and the indirect effects of aerosols affect the SST 174
gradients and favor drying at the northern edge of the ITCZ 175
[*Biasutti and Giannini*, 2006]. By contrast, for *Kim et al.* 176
[2010] aerosol radiative forcing and induced circulation 177
and precipitation cool the Sahel and the southern part of 178
Sahara desert more than the adjacent areas to the north and 179
south. It tends to shift the peak of the meridional temperature 180
gradient northward and consequently the African easterly jet. 181

[10] In their detailed review of biophysical processes 182
studies for the Sahel area, *Xue et al.* [2004] present the main 183
land/atmosphere feedbacks and mechanisms exerting a sig- 184

185 nificant impact on the Sahel climate (see *Xue et al.*'s [2004]
 186 Figure A42 and comments on their page 74 for more de-
 187 tails). In particular, as *Zeng et al.* [1999] show, they exhibit
 188 that interactive vegetation processes must be included in
 189 models for simulating correctly the decadal precipitation
 190 variability over the Sahel. Moreover, as *Charney et al.*
 191 [1977] and *Walker and Rowntree* [1977] show, *Xue et al.*
 192 [2004] highlight that increases/decreases in albedo lead to
 193 the reduction/augmentation in precipitation while less initial
 194 soil moisture leads to less precipitation.
 195 [11] About global warming, *Paeth and Hense* [2004],
 196 among other authors, have implied greenhouse-gas driven
 197 signals, showing that the partial amelioration of the Sahel
 198 drought in recent years may be a sign of a long-term
 199 increase in rainfall. For *Polyakov et al.* [2010], also, the
 200 current North Atlantic warming is linked to both this mul-
 201 tidecadal variability and long-term climate change (includ-
 202 ing anthropogenic and natural).

203 3. Data and Methods

204 3.1. SST Data

205 [12] The SST data are a 60°N–40°S selection of the
 206 extended reconstructed sea surface temperature (ERSST)
 207 from the most recently available Comprehensive Ocean-
 208 Atmosphere Data Set (COADS) SST data with improved
 209 statistical methods allowing stable reconstruction using
 210 sparse data. We will use the ERSST.v3b version which is an
 211 improved extended reconstruction over version 2 with no
 212 satellite data (more details available from *Smith et al.* [2008]
 213 and at [http://www.ncdc.noaa.gov/oa/climate/research/sst/](http://www.ncdc.noaa.gov/oa/climate/research/sst/ersstv3.php)
 214 [ersstv3.php](http://www.ncdc.noaa.gov/oa/climate/research/sst/ersstv3.php)). Computations of the derived SST signals of
 215 global and regional scale will be presented in section 3.1.

216 3.2. Rainfall Data

217 [13] The Sahel rainfall index used in this study is the
 218 precipitation anomaly defined by the NOAA NCDC Global
 219 Historical Climatology Network. This index refers to the
 220 1950–1979 climatology and is averaged over a 20°–10°N,
 221 20°W–10°E West African window (see jisao.washington.edu/data/sahel
 222 for more details). The correlation coefficients
 223 between the July–September values of this rainfall index and
 224 other Sahel indices used in the literature, such as those
 225 defined by *Lamb* [1978], *Bell and Lamb* [2006] and
 226 *Nicholson* [1979] are positive and significant at $p = 0.01$
 227 regarding to a Monte Carlo procedure taking into account
 228 autocorrelation in the series: $r = 0.89$ with the Nicholson's
 229 Sahel index over the common period 1901–1994 and $r =$
 230 0.58 with the Lamb's time series over the common period
 231 1941–2009.

232 [14] In addition, two data sets have been selected for
 233 enlarging the window: (1) the high-resolution CRU TS 2.1
 234 data set to focus more on different West African subregions:
 235 these data comprise 1224 grids of observed climate, for the
 236 period 1901–2002, and cover the global land surface at
 237 0.5 degree resolution [see *New et al.*, 2002; *Mitchell et al.*,
 238 2004; (2) the last available version of the VASCLimO 50-Year
 239 data set (1951–2000) from the Global Precipitation Clima-
 240 tology Centre (GPCC), because only this version supplies
 241 gridded time series of monthly precipitation at 1 degree
 242 resolution for climate variability and trend studies [*Beck et al.*,
 243 2005]: it is based on data selected with respect to a (mostly)

complete temporal data coverage and homogeneity of the 244
 time series (<http://gpcc.dwd.de>). 245

3.3. Atmospheric Data 246

[15] Two regional atmospheric signals representative of 247
 the African monsoon circulation in July–September have 248
 been defined between 20°W and 30°E through the NCEP/ 249
 NCAR reanalyses over the period 1950–2008: (1) the ver- 250
 tical velocity at 400 hPa (Pa/s) over 15°N–10°N (ω , the 251
 vertical velocity in Pa/s) which is directly linked to moist 252
 convection processes at Sahelian latitudes; (2) the West 253
 African Monsoon Index (WAMI) [*Fontaine et al.*, 1995] 254
 between 15°N and 5°N which is a proxy of the monsoon cell 255
 intensity at regional scale: WAMI is the difference between 256
 the standardized values of the wind modulus at 925 hPa and 257
 of the zonal wind at 200 hPa averaged in the considered 258
 domain. 259

[16] In addition, the atmospheric moisture flux at 950 hPa 260
 and the divergent (irrotational) part of the horizontal wind at 261
 the different pressure levels of the troposphere have been 262
 computed through the monthly NOAA-CIRES 20th Century 263
 Reanalysis. This data set is based on surface pressure 264
 observations assimilated every 6 h in an atmospheric model, 265
 and time-evolving sea surface temperature and sea ice 266
 concentration fields as boundary conditions. The model used 267
 the state-of-the-art atmospheric general circulation model, a 268
 2008 updated experimental version of the atmospheric 269
 component of NCEP's operational Climate Forecast System 270
 model [*Saha et al.*, 2006]. It has a spatial resolution of 271
 nearly 200 km in the horizontal (corresponding to a trun- 272
 cation T62) and 28 vertical levels. The data are provided at a 273
 $2^\circ \times 2^\circ$ latitude–longitude resolution (more details are pro- 274
 vided by *Compo et al.* [2006] and at [http://www.esrl.noaa.](http://www.esrl.noaa.gov/psd/data/gridded/data.20thC_ReanV2.html) 275
[gov/psd/data/gridded/data.20thC_ReanV2.html](http://www.esrl.noaa.gov/psd/data/gridded/data.20thC_ReanV2.html)). The data 276
 set will be used over the period 1920–2008 to limit time 277
 variations of the information anisotropy at the very begin- 278
 ning of the century and during the first world war. 279

3.4. Statistical Methods 280

[17] Statistical links are presented through linear correla- 281
 tions, multiple regressions, composite methods and cluster 282
 analyses. The correlation significance is estimated through 283
 permutation tests which do not require specific distributions 284
 such as normality and give more accurate P values than 285
 usual statistical tests. Correlation and P values at 0.05 and 286
 0.01 will be indicated in text and tables by one and two 287
 asterisks, respectively. Multiple regressions have been con- 288
 ducted with cross validation techniques. Composite results are 289
 tested using paired Student t test. Cluster analyses use a 290
 k-means algorithm minimizing the sum, over all clusters, 291
 of the within-cluster sums of point-to-cluster-centroid 292
 distances: each procedure has been repeated 100 times, 293
 each time with a new set of initial centroids. 294

4. Correlation Patterns 295

[18] Let us recall first the basic SST-Sahel correlation 296
 patterns observed over different periods at quasi-global 297
 scale: 1900–1949, 1950–1970, 1971–1990 and 1991–2008 298
 (Figure 1). During the first half of the 20th century (Figure 1a), 299
 a few Oceanic regions exhibit a statistical link with the 300
 Sahelian rainy seasons, i.e., the equatorial, southern and NW 301

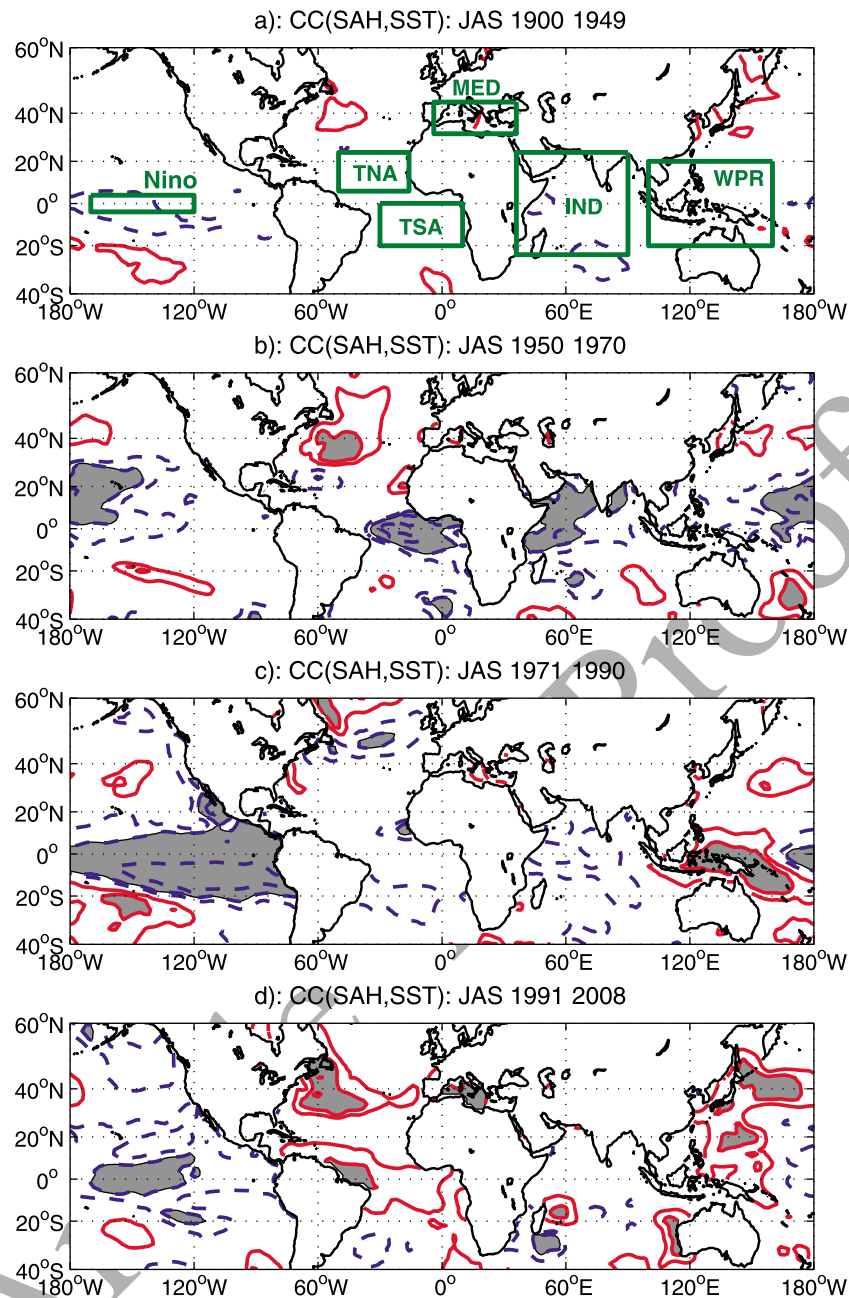


Figure 1. Temporal correlation coefficients between the Sahel rainfall index and the quasi-global SST field in July–September for different subperiods: (a) 1900–1949, (b) 1950–1970, (c) 1971–1990, and (d) 1991–2008. Values above 0.31 (~10% of common variance) are displayed in blue (red) contours for the negative (positive) values with a 0.2 interval; shadings are superimposed when they exceed 0.51. The green boxes in Figure 1a indicate the Oceanic regions used for defining the SST regional indices presented in section 5.

302 zones in the Pacific, some areas in the extratropical Atlantic
 303 in the Indian Ocean, along with the whole Eastern Medi-
 304 terranean and Black Sea. Interestingly, no signal is
 305 encountered in the tropical Atlantic.

306 [19] After 1950 (Figures 1b–1d), the coefficients increase
 307 and involve larger oceanic regions in the tropics, such as the
 308 eastern and central parts of equatorial Pacific, the Indian
 309 Ocean and the eastern Atlantic (negative correlations), the
 310 western equatorial Pacific, the western equatorial Atlantic

and the Mediterranean (positive correlations). In the extra- 311
 312 tropical region, positive coefficients are also registered by 313
 40°N in the Pacific and Atlantic.

[20] In fact, Figure 1 illustrates well the time instability of 314
 correlation patterns and reveals that changes at basin scale 315
 are obvious everywhere. Thus, the negative correlations 316
 observed in the 1950s and 1960s (Figure 1b) in the equa- 317
 torial Atlantic and Indian Ocean, disappear in the 1970s and 318
 1980s (Figure 1c) and become positive on the most recent 319

320 period (Figure 1d). It is thus interesting to separate this
321 quasi-global evolution from proper SST variability in the
322 different basins. There are several ways for doing that.

323 [21] In this study, a quasi Global SST (GSST) index,
324 weighted by the square root of cosine of latitudes and
325 averaged between 60°N and 40°S is first defined as an
326 Oceanic proxy of the global SST evolution. $GSST_{(time)} =$
327 $\Sigma (SST_{(lat,lon,time)} \cdot \cos(lat)^{0.5}) / n$, where n is the number
328 of grid points considered. The GSST influence is then
329 removed to each line to better capture regional signals
330 that can be considered as independent from global evo-
331 lution: $SST'_{(lat,lon,time)} = SST_{(lat,lon,time)} - GSST_{(time)}$. Such
332 a procedure is more natural and appropriate than remov-
333 ing a simple linear trend not observed over the reference
334 period. Although GSST is defined at a monthly scale, its
335 long-term evolution (see Figure 2a and its caption) is
336 similar to the GW signal based on yearly averaged global
337 SSTs, between 60°N and 45°S because of lower SST data
338 coverage, shown by *Mohino et al.* [2011].

339 5. Time Evolution of Key SST Regional Indices 340 Versus Sahel Rainfall

341 [22] Nine regional SST indexes representative of the
342 regions linked to Sahel rainfall variability (Figure 1) are
343 now defined as a snapshot of SST evolution since 1900,
344 by averaging the values over: (1) the western Mediterra-
345 nean (WMED: 32°N–44°N; 6°W–15°E) and eastern
346 Mediterranean (EMED: 32°N–44°N; 15°E–36°E) basins,
347 and the whole Mediterranean (MED); (2) the northern
348 tropical Atlantic (TNA: 5°N–24°N; 50°W–15°W), the
349 southern tropical Atlantic (TSA: 20°S–0°; 30°W–10°E) and
350 the TNA-TSA differences. The correlation between TSA
351 and an equatorial Atlantic index computed over (3°N–3°S
352 and 20°W–0°) is positive, high and significant ($r =$
353 $+0.86^{**}$); and (3) the tropical Indian Ocean (IND: 24°S–24°N;
354 35°E–90°E), the west Pacific Region (WPR: 20°N–20°S;
355 100°E–160°E) and the Nino 3.4 region (Nino: 5°S–5°N;
356 170°W–120°W).

357 [23] Finally a detrended and unsmoothed version of the
358 Atlantic Multidecadal Oscillation (AMO) is added since
359 *Goldenberg et al.* [2001], *Zhang and Delworth* [2006] and
360 *Polyakov et al.* [2010], among others, have shown the role
361 of AMO on observed multidecadal variations of SSTs and
362 Sahel rainfall. We use the NOAA PSD AMO, from the
363 Kaplan SST data set V2 (5 × 5) referring to the area
364 weighted average over the North Atlantic (0°–70°N).

365 [24] Figure 2 presents time variability of these SST signals
366 since 1860 with superimposed July–September Sahelian
367 rainfall time series since 1900. The quasi global SST field
368 evolution (GSST in Figure 2a) is marked by two major
369 warming phases occurring from 1910 to 1940, then from
370 1975 to present. Notice that the AMO time series (thin
371 curve) which describes an apparent 60–80 year pseudocycle
372 in SSTs displays prolonged periods of warming and cooling
373 often in phase and correlated with GSST ($r = +0.57^{**}$).

374 [25] In the Mediterranean, SST evolutions in the western
375 and eastern basins (WMED, EMED dashed and solid curves
376 in Figure 2b) exhibit marked covariations in the last 50 years
377 with a noticeable cooling from 1960 to 1980 concomitant of
378 the Sahelian dry phase (bars) followed by a clear warming,
379 concomitant of the recent Sahel rainfall recovery. In fact,

EMED remains positive (negative) from 1912 to 1970 (1970
to 1997) during the long period of Sahelian rainfall excess
(deficit).

[26] In the tropical Atlantic (Figure 2c) the northern
(dashed curve) and Southern (solid curve) anomalies exhibit
often inverse polarities as in years 1917–1925, 1950–1960,
1967–1975 which can favor interhemispheric SST anomaly
gradient able to modify the location of the ITCZ. This
inverse evolution, associated with the dipolar pattern
between the northern and southern basins is well captured
by the TNA-TSA difference (circles).

[27] SST evolutions in the Indian and Pacific oceans
(IND, Nino and WPR in Figure 2d) also show a strong
variability all along the period. In particular the IND series
(solid curve) displays a succession of years with negative
values (1925–1960) followed by a warm phase since 1960,
while the Nino (curve with circles) and WPR (dashed curve)
series are negatively correlated all along the period ($r =$
 -0.72^{**}). This inverse correlation is due to the well-known
El Niño–Southern Oscillation seesaw of reversing surface
air pressure between the eastern and western tropical Pacific.

[28] Let us now display in Table 1 the significant corre-
lation coefficients registered between these SST indexes and
rainfall amounts over different African regions, i.e., the
western, central and eastern parts of the Sahelian (10°N–20°N
and Guinean (5°N–9.5°N) belts. The results show that (1) the
Sahelian belt is more affected by the teleconnection than the
subequatorial zone, (2) connections imply nearly all indexes
except AMO and TNA, and (3) small differences are recorded
between the western, central and eastern African windows.
Overall, correlations are negative, except those implying the
Mediterranean basins, and the equatorial/southern tropical
Atlantic. This is well confirmed through composite analyses
(Table 2) retaining only the SST anomalies exceeding 10.51
standard deviation over a larger period (1900–2008).
Noteworthy, the teleconnection is rather linear but stronger
with the Mediterranean index (correlated positively in 76%
of occurrences), and with IND (70%) and Nino (63%), both
correlated negatively with Sahelian rainfall. In the Atlantic
TSA exhibits a negative relationship in 57% of occurrences.

6. Time Instability of the SST-Sahel Teleconnection

[29] To better focus on this aspect, already noticed in
Figure 1 and section 4, Figure 3 displays 20 year running
correlations registered with each SST index. Several ob-
servations may be made.

[30] 1. The GSST and AMO series change continuously
and are significant in less than 10% of occurrences: with
GSST correlation series (bold curve in Figure 3a) often
negative in the 1960s, 1970s and 1980s, i.e., a period of
increasing drought occurrences over Sahel in agreement
with *Giannini et al.* [2003]. The lack of correlation with
AMO is not surprising regarding the period and *Hodson*
et al. [2010], who show that, in contrast to some studies,
the Atlantic Multidecadal Oscillation was not the primary
driver of recent reductions in Sahel rainfall. However, sig-
nificant correlations are observed in the 50s, and are con-
sistent with a northward displacement of the ITCZ and wet
anomalies in the Sahel [*Mohino et al.*, 2011].

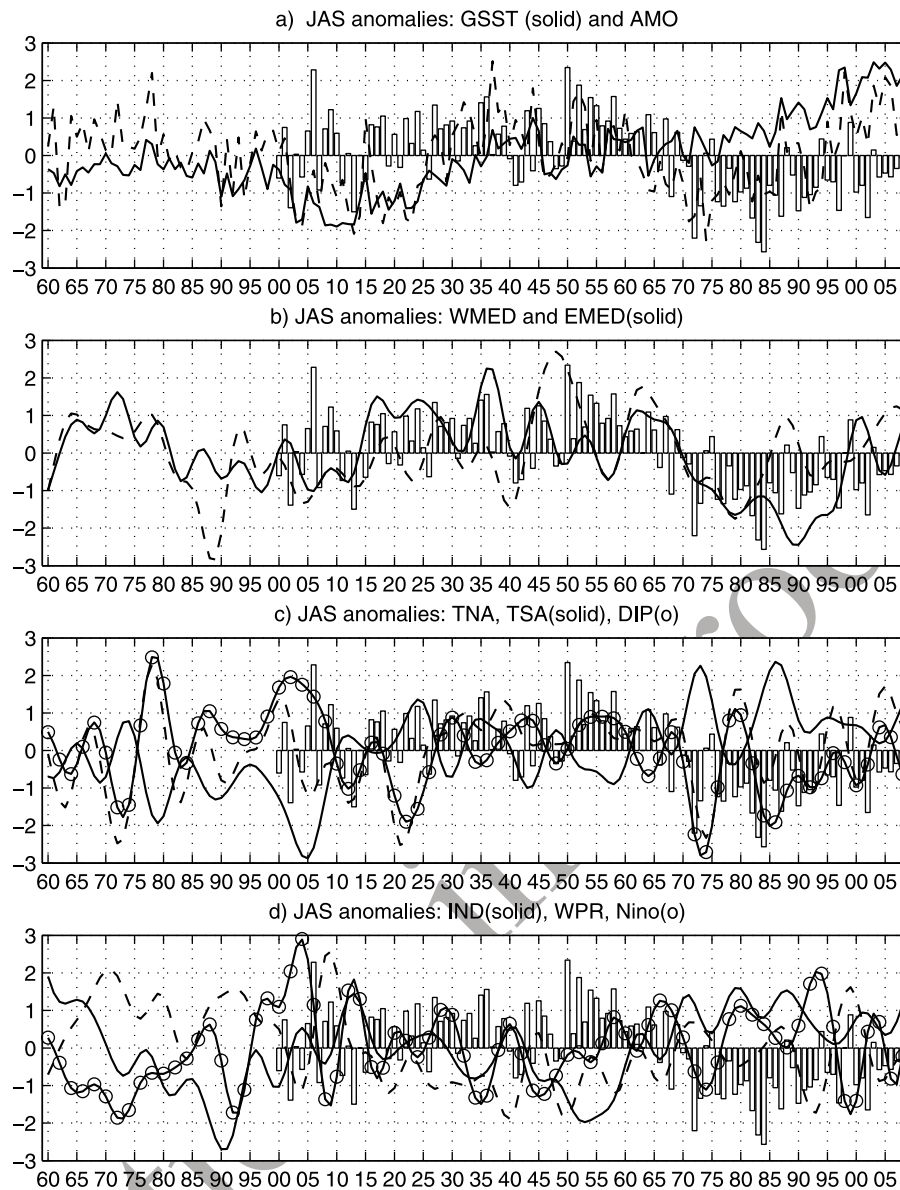


Figure 2. Time evolution of the July–September standardized time series of Sahel rainfall (bars) on the period 1900–2008 and of a few selected low-frequency SST anomaly indices (superimposed curves) over the period 1860–2009. (a) Atlantic Multidecadal Oscillation (AMO, dashed curve) and near global SSTs (GSST, solid curve); details in sections 4 and 5. (b) Western (dashed curve) and eastern (solid curve) Mediterranean SSTs: WMED (32°N–44°N; 6°W–15°E) and EMED (32°N–44°N; 15°E–36°E). (c) Tropical northern (dashed curve) and southern (solid curve) Atlantic SSTs: TNA (5°N–24°N; 50°W–15°W) and TSA (20°S–0°; 30°W–10°E) along with the TNA–TSA difference (dash-dotted curve with circles). (d) Indian (IND, solid curve), Nino 3.4 (solid curve with circles), and west Pacific region (WPR) (dash-dotted curve with circles) SSTs: IND (24°S–24°N; 35°E–90°E), Nino3.4 (5°S–5°N; 170°W–120°W), and WPR (20°N–20°S; 100°E–160°E). In Figures 2b–2d, quasi-decadal/multidecadal SST signal have been isolated from higher frequencies using a zero-phase forward and reverse digital filtering [Murakami, 1979] for eliminating time variability < 8 years at each grid point of the weighted SST anomaly field.

439 [31] 2. The relationship involving WMED is rather low
 440 and rarely significant (13%); it is significant in the 1960s
 441 and 1970s then after 1982 (thin curve, Figure 3b). In con-
 442 trast, except in the 1940s and 1950s, EMED (bold curve,
 443 Figure 2b) shows a quasi-persistent teleconnection in more

than 50% of years. The teleconnection is in good agreement
 444 with work by Rowell [2003], Raicich et al. [2003] and
 445 Fontaine et al. [2009], who showed observational and
 446 model evidence of a thermal forcing of the Mediterranean–
 447 with maximum amplitude in the eastern basin—on the African
 448

Table 1. Significant Correlation Coefficients ($\times 100$) Between SST Indexes and CRU Rainfall Averaged in the Sahelian (SAH, 10°N – 20°N) and Guinean (GUI, 5°N – 9.5°N) Belts Computed Over the Period 1950–2002 and in the Western (15°W – 0°), Central (0° – 15°E), and Eastern (15°E – 30°E) Longitudes^a

	Western Region		Central Region		Eastern Region	
	SAH	GUI	SAH	GUI	SAH	GUI
GSST	–52*				–35*	
AMO						
WMED	+44**		+40**			+35*
EMED	+48**		+54**		+43**	+31*
TNA						
TSA	–35*	+35**	–42**	+35**	–35*	–34*
IND	–53**	–29*	–45**		–37*	
NINO	–30*		–29*		–34**	–40**

^aSignificance at $p = 0.05$ and 0.01 denoted by one and two asterisks, respectively.

monsoon leading to increasing moisture convergence (and therefore rainfall) over Sudan-Sahel latitudes through changes in the southward moisture advection across the eastern Sahara by the flow.

[32] 3. The connection with TNA is rarely significant (4%) and only observed during the wet 50s and 60s (dashed curve in Figure 3c). The negative correlation with TSA is more recurrent (20%), primarily in the 1940s–1970s. As a result, the association with the dipolar pattern is positive and significant during the same period (15%, dash-dotted curve with circles). This is in good agreement with *Janicot et al.* [2001] who showed that during the transition between the wet sequence to the dry one, the correlations between the Sahel rainfall and the tropical Atlantic dipole were the highest.

[33] 4. The statistical relationship with IND and Nino is negative. Figure 3d shows that the correlation is more often significant with IND (47%, chiefly between 1920 and 1975) than with Nino (28%, mainly from 1900 to 1930, and after 1968). Indeed, IND and Nino are not significantly correlated together over the total period ($+0.13$) or over subperiods before/after the 1976–1977 climate shift in the tropical Indian-Pacific region ($+0.12$ and $+0.13$, respectively). The correlation with Nino confirms results of *Joly and Voldoire* [2009] and *Rodríguez de Fonseca et al.* [2011] and is partly due to the Atlantic Niño–Pacific La Niña relationship starting after the 1970s found by *Polo et al.* [2008] and *Rodríguez-Fonseca et al.* [2009]. It is also noteworthy that the 20 year running mainly deemphasizes the information in past 20 years, which is an important rainfall recovery period. Figure 2, which only eliminates the time variability < 8 years, clearly

show that the Indian Ocean SST variability fails to catch the recovery trend. The 20 year running mean tends to make Indian SST correlation artificially high over the recent period. Figure 2c shows also that Atlantic Ocean SST catches well the recovery after the 1980s. The statistical link with WPR is positive (Figure 3d) and significant (9%, mainly between the end of the 1960s and the mid-1980s).

[34] Finally, two conclusions must be drawn: (1) there is no empirical evidence of correlation stability between the selected SST indices and Sahelian rainfall at the decadal or multidecadal scales, and (2) only the eastern Mediterranean and Indian Ocean SST series show significant correlations in about 50% of years. Another striking result is that correlations with the different oceanic basins do not occur in the same periods. Thus the anomalous wet July–August–September seasons observed during the 1940s, 1950s and 1960s are mostly associated with (1) colder SST anomalies over the Indian Ocean (IND) and (2) warmer (colder) SSTs over the TNA (TSA) basins, which induces a northward SST anomaly gradient in the tropical Atlantic. By contrast, the drought phase following the 1960s appears to be linked to (1) colder waters in the eastern Mediterranean and in the western tropical Pacific, and to (2) Nino episodes in the central–eastern Pacific (Figure 3), compatible with the Atlantic Niño–Pacific La Niña relationship observed after the 1970s by *Polo et al.* [2008] and *Rodríguez-Fonseca et al.* [2009]. It is also interesting to mention that the Indian ocean is not (is) significantly correlated with Sahelian rainfall when Sahelian rainfall is (is not) linked with Nino.

7. Linear Regression and Clustering

[35] Studying the summer Sahel-ENSO teleconnection, *Janicot et al.* [2001] over the period 1945–1993 showed that the decadal-scale SST variations weakly affect Sahel rainfall variability but that they induce an indirect effect on Sahel rainfall by enhancing the impact of the warm ENSO phases after 1980, through an increase in the fill-in of the monsoon trough and a moisture advection deficit over West Africa. Interestingly, they pointed out an adjustment in correlation after the mid-1970s (1975–1980) due to the jump in SST observed for this period in the Pacific and Indian oceans. On the basis of our results this hypothesis can be completed since no abrupt change alters the IND and Nino series used here (Figure 2d). Moreover the SST indices document other oceanic basins (section 2) over a larger period (1950–2008). It is therefore interesting to analyze first the summer Sahel-SST teleconnection in a more global context for quantifying the relative weights of the global (GSST) versus SST indices of regional extent in their relationship with Sahelian rainfall

Table 2. Contingency Table Between the Sign of the Sahel Rainfall Index (SAH⁺, SAH[–]) and Values of SST Indexes Below -0.5 Standard Deviations (Cold Situations) or Above $+0.5$ Standard Deviations (Warm Situations) in Selected Basins^a

	TNA		TSA		DIP		MED		IND		NINO	
	< -0.5	$> +0.5$	< -0.5	$> +0.5$	< -0.5	$> +0.5$	< -0.5	$> +0.5$	< -0.5	$> +0.5$	< -0.5	$> +0.5$
SAH ⁺	26%	22%	25%	22%	27%	27%	13%	38%	40%	14%	31%	18%
SAH [–]	28%	25%	22%	32%	24%	22%	38%	12%	16%	30%	19%	32%

^aSelected basins: TNA, tropical northern Atlantic; MED, Mediterranean; TSA, tropical southern Atlantic; DIP (= TNA-TSA), Atlantic dipole; NINO, equatorial eastern Pacific; IND, Indian Ocean. The values are expressed in percentages of occurrences (the sum of four percentages for each Ocean basin is 100%). Values $> 30\%$ are boldface. Period is 1900–2008.

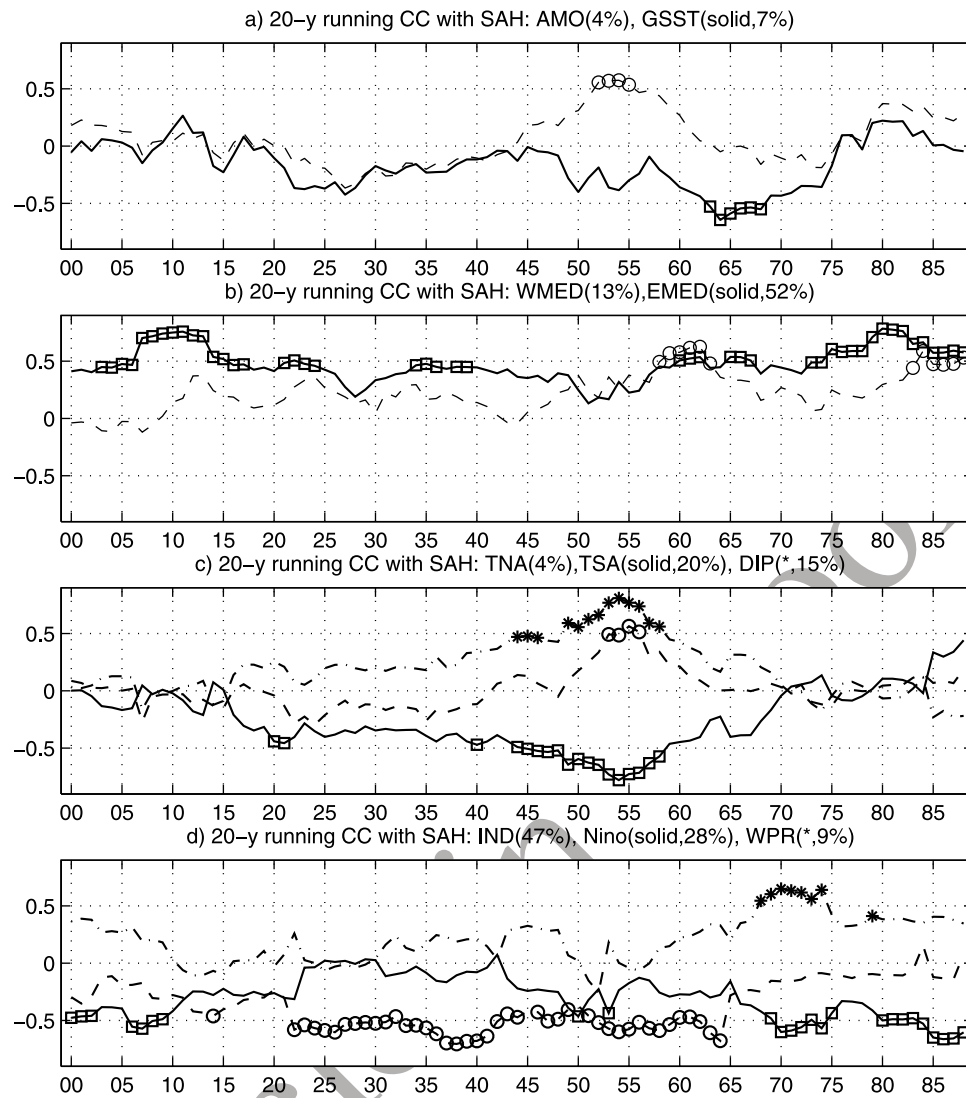


Figure 3. Correlation coefficients computed on 20 year running windows between the Sahel rainfall index and the SST indexes displayed in Figure 2. The x axis is labeled with the first year of the 20 year period, so 1900 means 1900–1919. Symbols are superimposed when the values are significant regarding significance tests based on permutation resamples drawn at random from the original data and Monte Carlo procedure. Panels are as in Figure 1. The titles indicate the relative percentage of significant values on the period, 1900–2008.

528 and African monsoon intensity. This is also supported by the
529 fact that Pacific-Niño, Atlantic La Niña and cooling of the
530 western Indian Ocean have, from the 1970s, an atmospheric
531 response related to changes in the Walker circulation
532 [Rodríguez de Fonseca et al., 2011].

533 [36] For determining these weights and their time evo-
534 lution, we estimate Sahel rainfall and the African mon-
535 soon intensity as depicted by the WAMI and ω indexes
536 (section 2.3), through linear multiple regressions after step-
537 wise selections of 4 SST indices and cross validation over
538 different periods. Table 3 displays both the correlation sta-
539 tistics and the vectors of regression coefficients (see the
540 legend for more details) explaining the highest part of var-
541 iance. Sources of skill are found in both the quasi-global
542 (GSST) and regional SST variability with high and signifi-
543 cant correlations. Notice however that over the period 1950–

2008, the statistical impact of GSST variability explains a
544 smaller part of the relationship with Sahelian rainfall or the
545 African monsoon cell (WAMI) than basin-scale variability.
546 By contrast the GSST coefficients are higher with the ver-
547 tical velocity averaged above the Sahel belt ($-\omega$). Compared
548 to the period 1950–1979, recent years are marked by a
549 decrease in the teleconnection over the southern tropical
550 Atlantic and the Indian Ocean and an increase over the
551 Mediterranean and Niño areas and also with global warm-
552 ing. Overall the Mediterranean SST series registers clearly
553 the strongest coefficients (italicized values in Table 3) with
554 the Sahel rainfall and the African monsoon cell (WAMI).
555

[37] We present now an objective cluster partition of SST
556 series for analyzing better the structure of statistical
557 dependencies between basin-scale indexes, using a k-means
558 algorithm minimizing the sum, over all clusters, of the
559

Table 3. Linear Multiple Regression (LMR) Estimating the July–September Sahel Rainfall Amounts and Two African Monsoon Descriptors (WAMI and $-\omega$) After Stepwise Selections of the Best Four SST Indices^a

	R	Rev	Racv	GSST	TSA	MED	IND	NINO	Area
	<i>SAHEL</i>								
1950–2008	+84	+79	+59	–34	–22	+54	–37		
1950–1979	+91	+88	+72		–44	+45	–37	–15	
1980–2008	+81	+67	+32	+03		+65	–17	–40	
	<i>WAMI</i>								
1950–2008	+72	+66	+39	–23	–34	+38	–32		
1950–1979	+74	+64	+28	+19	–38	+42	–31		
1980–2008	+89	+84	+65	+38	–24	+48		–39	
	$-\omega$								
1950–2008	+67	+60	+30	–40	–26	+30	–23		
1950–1979	+66	+48	+06	+19	–31	+49	–14		
1980–2008	+85	+77	+51	+49	–15	+32		–44	

^aSee section 2 for more information on WAMI and $-\omega$. All the series have been standardized before applying the procedure ensuring easier comparisons. R Rev Racv, total correlation (R), correlation after cross validation (Rcv), and adjusted correlation after cross validation (Racv). GSST, TSA, MED, IND, and NINO area: the vector of regression coefficients ($\times 100$) in the linear model (highest value in bold). Italics denote strongest coefficients. Three periods are considered: 1950–2008, 1950–1979, and 1980–2008.

within-cluster sums of point-to-cluster-centroid distances. The procedure is applied over the period 1900–2008 on 5 regional SST indices after standardization of the series: the Mediterranean, the northern and southern tropical Atlantic, the Indian Ocean and the eastern equatorial Pacific. Several k numbers (2 to 4 classes) have been tried and we report only those with k = 3 and 2 which can be estimated as the most efficient choice with respect to the number of variables and the length of the series.

[38] First lines of Table 4 display the associated cluster centroid locations from a three-cluster partition, while Figure 4a shows the projection of results onto the rainfall series.

[39] 1. The “white” cluster (see white bars in Figure 4 and first row in Table 4) is associated with a mean SST pattern (occurrence: 34%) controlled by a cold/warm evolution in the tropical Atlantic (TNA/TSA) where warm TSA dominates, and a Nina-like growth in the Pacific, in agreement with *Rodríguez-Fonseca et al.* [2009]. This type taking into account the inverse SST progressions in the southern Atlantic and in the equatorial eastern Pacific, will be called AP (Atlantic-Pacific). Noteworthy, this cluster is strongly linked to Sahel rainfall variability.

[40] 2. The “blue” cluster (blue bars in Figure 4 and second row in Table 4) is more frequent (40%) and clearly associated with Sahel rainfall excesses. It designates a situation where a Mediterranean warming is concomitant of warm/cold evolutions in the Atlantic with cooling over the southern Atlantic and the Indian Ocean. This cluster is therefore named MAI (Mediterranean-Atlantic-Indian).

[41] 3. The “red” cluster (bars in Figure 4 and third row in Table 4) is less frequently observed (26%) but clearly occurred during the dry Sahelian phase in the 1970s and 1980s. It associates a Mediterranean cooling with a warming in the Indian and in the equatorial eastern Pacific (Nino-

type), despite the low correlation between IND and Nino time series (section 3.3). This cluster named MIP (Mediterranean-Indian-Pacific) requires hence mechanisms linking the Indian and Pacific basins such as those illustrated by *Annamalai et al.* [2005] and *Izumo et al.* [2010]. It is independent of SST variability in the Atlantic.

[42] Let us now concentrate on the coevolutions of Sahel rainfall (Figure 4b) and cluster occurrences over successive 10 year periods between 1900 and 2008 (Figure 4c). Three points emerge: (1) the strong decadal variability affecting MAI occurrences; (2) their negative correlation with MIP; and (3) the resulting inverse relationship with rainfall anomalies. For example, the progressive increase/decrease of MAI/MIP occurrence in the first part of the last century is accompanied by a long-term rise in Sahelian rainfall. Similarly, the Sahelian transition between the wet 1950s and dry 1970s and 1980s is synchronous of a complete MAI vanishing and of a moderate MIP increase, while the partial recovery in the 1990s is concomitant of the reverse. This inverse relationship involving MAI and MIP occurrences proves that the major role in the teleconnection is played by inverse thermal evolutions between the Mediterranean and Indian Ocean, although correlations between SST values averaged over these two basins are low (–0.23, –0.31 and +0.20 for the periods 1900–2008, 1950–1979 and 1980–2008). Regarding Sahelian rainfall, the opposite thermal evolution in the Mediterranean and Indian Ocean is also in good agreement with recent studies focusing on the mechanisms involved in the Indian Ocean and in the Mediterranean. *Bader and Latif* [2011] recently showed that the warming of the Indian ocean is related to a rainfall decrease over the Sahel, while *Fontaine et al.* [2009] and *Gaetani et al.* [2010] showed that the Mediterranean warming is related to a rainfall increase over the Sahel.

[43] The results from a partition into two clusters are displayed in Figure 4b and Table 4. They confirm that, situations including (excluding) opposite thermal evolution in the Mediterranean and in the Indian Ocean are (are not) associated with significant Sahelian rainfall anomalies. Additionally, the scatterplot presented in Figure 5 allows us to compare the statistical impact of inverse SST evo-

Table 4. Cluster Centroid Locations, and Percentages of Occurrence, of Partitions in Three and Two Clusters Based on Squared Euclidean Distances Between the Standardized SST Time Series Over the Period 1900–2008^a

Clusters and Percent Occurrence	MED	TNA	TSA	IND	Nino Area
<i>Three-Cluster Partition With Five SST Series (See Figure 3a)</i>					
White (34%)	+0.02	–0.40	+0.70	–0.06	–0.73
Blue (40%)	+0.60	+0.33	–0.60	–0.61	+0.12
Red (26%)	–0.97	+0.01	+0.02	+1.03	+0.78
<i>Two-Cluster Partition With Five SST Series (See Figure 3b)</i>					
Blue	+0.56	+0.26	–0.49	–0.61	–0.10
Red	–0.51	–0.24	+0.45	+0.56	+0.09

^aMED, Mediterranean; TNA and TSA, northern and southern tropical Atlantic; IND, Indian Ocean; Nino, eastern equatorial Pacific. The k-means algorithm has been repeated 100 times, each time with a new set of initial centroids, ensuring that the convergence criterion is met (the assignment remains the same). Values higher than 10.51 are boldface.

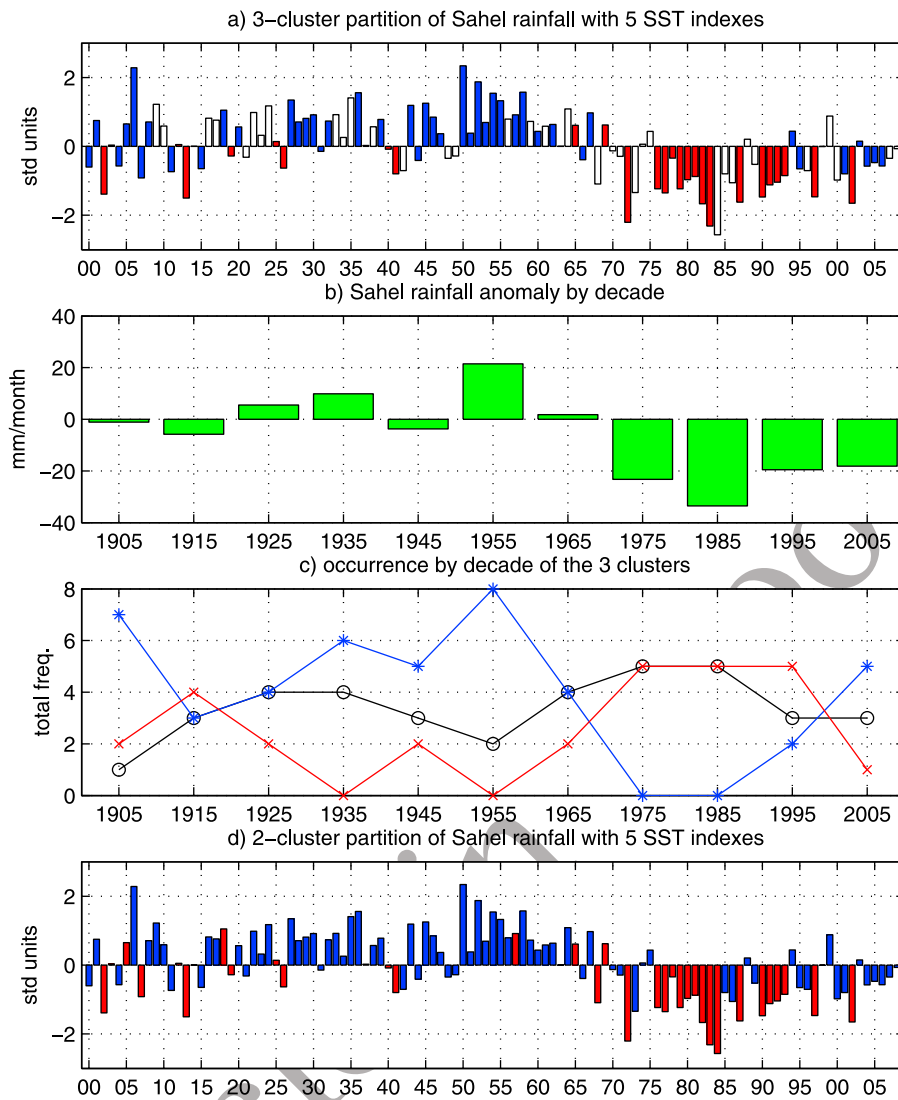


Figure 4. Time projections of (a and d) the k-means results displayed in Table 3 onto the standardized Sahel rainfall series at an interannual time step and (b and c) covariation with Sahel rainfall in mm/month over 10 year subperiods between 1900 and 2008: AP (white), MAI (blue), and MIP (red).

636 lutions between MED and IND (x axis) and TNA and TSA
 637 (y axis) on the Sahelian rainy seasons since 1901. The
 638 results show clearly that MED-IND differences discrimi-
 639 nate better rainfall anomalies than the meridional SST
 640 structure in the tropical Atlantic: more than two thirds of
 641 the rainy seasons classified as dry (wet) are concomitant of
 642 negative (positive) MED-IND differences, versus only 1 out
 643 of 2 with TNA-TSA differences. These scores reach 16 out of
 644 18 (12 out of 15) for the rainy seasons classified as very dry
 645 (very wet) versus only 10 out of 18 (10 out of 15) with the
 646 Atlantic dipole. This picture is in agreement with Raicich
 647 *et al.* [2003] results who found that a stronger than aver-
 648 age Indian monsoon has a positive impact on the Sahelian
 649 precipitation, through the eastern Mediterranean cyclonic
 650 circulation: cold anomalies in the Indian Ocean are favor-
 651 able to the monsoonal circulation over the Indian subcon-
 652 tinent, while warm anomalies in the Mediterranean enhance
 653 the cyclonic circulation; as a consequence the northerly flow

across the Sahara is strengthened and the precipitation over
 the Sahel is increased.

8. Impacts of MED-IND and TNA-TSA Thermal Contrasts

[44] The above statistical results show that the relationship
 between Sahelian rainfall and SST anomalies mostly implies
 the thermal variability observed over the Oceanic basins
 close to the African continent, especially the thermal con-
 trasts between (1) the Mediterranean and Indian Ocean, and
 (2) the northern and southern tropical Atlantic. This section
 is focused on these topics and on associated dynamics.

8.1. Precipitation Field and Atmospheric Moisture Flux in Low Levels

[45] The analysis refers to the well documented period
 1951–2000 (see section 2.1), marked by a positive phase of

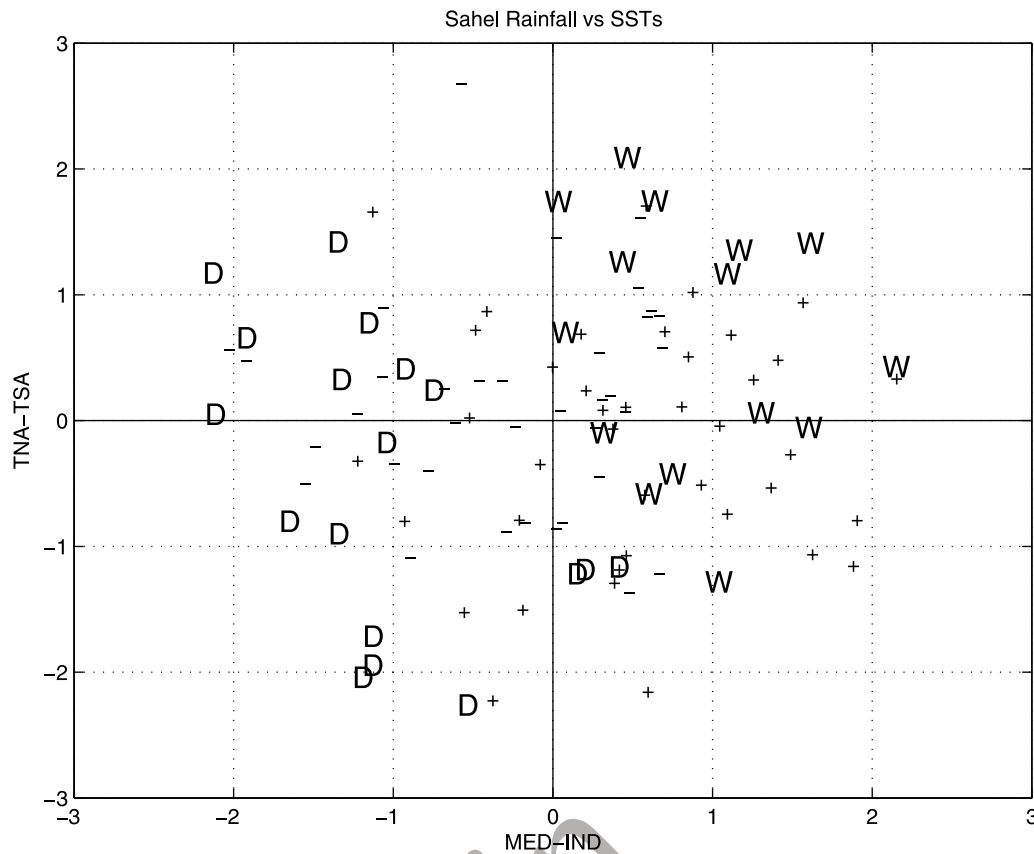


Figure 5. Scatterplot of summertime (July–August–September) Sahelian rainfall as a function of the differences computed between the MED and IND (x axis) and TNA and TSA (y axis) standardized time series. W (D) denote the wettest (driest) rainfall anomalies, i.e., those exceeding 1 standard deviation in absolute value, while pluses and minuses refer to other positive (negative) anomalies. Period is 1900–2008.

669 global warming in SST as previously shown in Figure 2a, in
 670 order to focus on the region bounded by 40°S and 50°N in
 671 latitude and 60°W and 60°E in longitude (Figure 6). An
 672 estimate of changes induced by linear trends in SSTs linked
 673 to global warming is also provided in Figure 6 (left) and
 674 Figure 6 (right), referring to calculations before and after,
 675 respectively, removing the linear trends in SSTs. It appears
 676 that such trends tend to increase the correlations but do not
 677 change neither the spatial signal at large scale, nor the
 678 preeminence of MED-IND variations against TNA-TSA
 679 variability. In fact, the former are synchronous of in phase
 680 rainfall anomalies over the whole Sudan-Sahel belt with
 681 areas of inverse polarity in Brazil and central Europa
 682 (Figures 6a and 6b) while the latter contrasts sub-Saharan
 683 regions (i.e., Northern Africa, Sahelian belt) to the equato-
 684 rial zone across the Atlantic (Guinean coast, north Brazil).
 685 They imply mechanisms of different scale: the Atlantic
 686 dipole impacts directly on the meridional structure of the
 687 rainbelt in the vicinity of the equatorial Atlantic. By contrast
 688 the larger action of MED-IND can be interpreted through
 689 the picture given by Raicich *et al.* [2003]: cold anomalies in
 690 the Indian Ocean favor the monsoonal circulation over the
 691 Indian subcontinent, while warm anomalies in the Medi-
 692 terranean strengthen the northerly flow across the Sahara,
 693 increasing precipitation over the Sahel .

[46] The basic relationship observed with the summertime
 atmospheric dynamics is now investigated using a subset of
 the monthly NOAA-CIRES 20th Century Reanalysis over
 the period 1920–2008 (for the reasons listed in section 2.3).
 We present the results from the moisture flux at 950 hPa
 because this field emphasizes the main elements of the
 monsoon circulation in low levels, in particular (1) the
 interhemispheric moisture transport along the eastern coast
 of Africa associated with the Indian monsoon and (2) the
 African monsoon circulation between the southern-equatorial
 Atlantic and the Sudan-Sahel belt (Figure 7a). Composites
 regarding SST differences between (1) the northern and
 southern tropical Atlantic basins and (2) the eastern Medi-
 terranean basin and the Indian Ocean are then computed.
 These differences are counted positive if $TNA-TSA > 0$ or
 $MED-IND > 0$.

[47] The results show that both SST indices are associated
 with an enhancement of the African monsoon circulation on
 the Atlantic and the African continent. However, their sta-
 tistical effect on the moisture transport is clearly different. A
 strong TNA-TSA dipole is associated with a reinforced
 southeasterly flux over the western equatorial Atlantic and
 with an enhancement of the southwest monsoon over the
 Sahelian belt (Figure 7b). By contrast, a positive MED-IND
 index reinforces the northerlies and southerlies over the

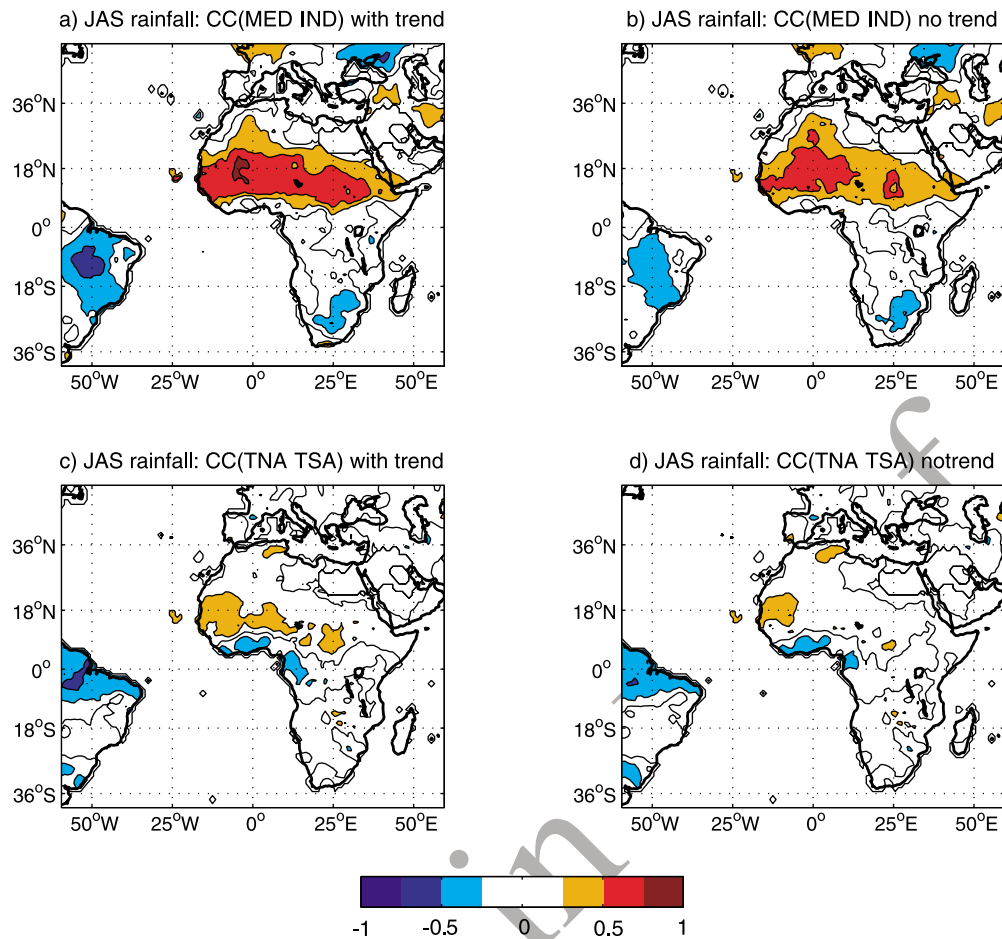


Figure 6. Correlation coefficients with the rainfall field in July–September using the Vaslimo SST data (period 1951–2000). Results obtained with SST differences defined between (a and b) the eastern Mediterranean and Indian basins and (c and d) the northern and southern tropical Atlantic with (Figures 6a and 6c) and without (Figures 6b and 6d) linear trends. Values below 0.251 are not displayed.

719 Atlantic (Figure 7c) and therefore the interhemispheric
 720 moisture flux convergence. In addition the northeasterly
 721 transport from the eastern Mediterranean and the southwest
 722 transport from the eastern equatorial Atlantic (i.e., the
 723 monsoon flow) are both strengthened: in agreement with the
 724 empirical and numerical results of Rowell [2003], Fontaine
 725 *et al.* [2009] and Gaetani *et al.* [2010] this can produce an
 726 anomalous poleward ITCZ extension.

727 8.2. Atmospheric Circulation

728 [48] We investigate now the atmospheric circulation in
 729 northern summer on the period 1920–2008 from (1) the
 730 vertical atmospheric motion ($-\omega$ in Pa s^{-1}) and (2) the
 731 divergent part (irrotational) of the horizontal wind (m s^{-1})
 732 which is proportional to the gradient of the velocity potential
 733 ($\text{m}^2 \text{s}^{-1}$). The use of the divergent horizontal wind removes
 734 any continuity problem when the circulation is averaged
 735 along the zonal and meridional directions. Notice also that
 736 computations have been made on the global field to avoid
 737 any bias.

738 [49] The meridional component of this circulation, averaged
 739 over the African longitudes (20°W – 40°E) is displayed in
 740 Figure 8a. It portrays the meridional overturning in the region,
 741 associated with the Hadley circulation. The monsoonal cir-

742 culation in low levels is marked here by the shift of air as-
 743 cents in low troposphere over Sudan-Sahel and by a small
 744 northerly component in midlevels, at the altitude of the
 745 African Easterly Jet (700–600 hPa). Since the meridional
 746 plane captures well these basic features, it is interesting to
 747 concentrate on changes induced by variations in MED-IND
 748 and TNA-TSA contrasts.

[50] The MED-IND composite (Figure 8b) exhibits clear
 749 ascents in low and mid levels around 40°N in relation to the
 750 warming of the Mediterranean basin. Southerly anomalies
 751 are noticed in all the troposphere between 45°N and 60°N
 752 while northerly departures prevail above 500 hPa over the
 753 20°N – 40°N latitudes. This denotes a region of divergence
 754 anomaly in upper levels in the northern subtropics (35°N –
 755 40°N). Southward, above the monsoon region, a general
 756 descent from midlevels toward the surface is evidenced
 757 above 10°N – 18°N and associated with rising motion above
 758 the Saharan thermal lows, i.e., at the latitude of the northern
 759 tropic. Above 500 hPa where moist convection develops,
 760 upward anomalies are present over the Sahelian belt.
 761

[51] The TNA-TSA composite (Figure 8c) is very differ-
 762 ent. The significant signals are mainly located in the south-
 763 ern hemisphere. Over northern Africa a general subsidence
 764 departure above 5°N is evidenced in the whole troposphere
 765

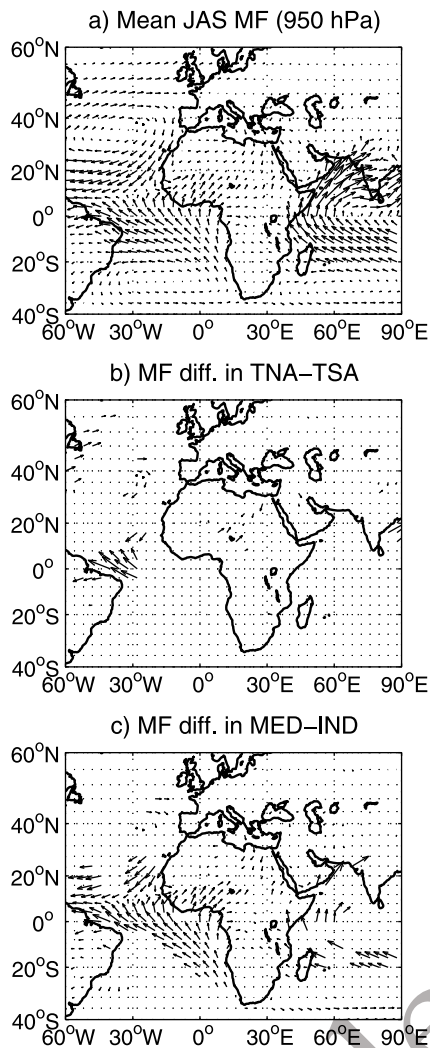


Figure 7. July–September moisture flux at 950 hPa over the period 1920–2008. (a) Mean values, (b) significant differences between the northern and southern tropical Atlantic basins, and (c) significant differences between the eastern Mediterranean basin and the Indian Ocean. The statistical significance has been estimated on the zonal and meridional components through a Student t test contrasting the 20 highest and the 20 lowest seasonal differences versus all the remainders.

766 whereas ascents prevail in mid and high levels south of
767 10°S. These opposed vertical anomalies are in agreement
768 with the rainfall contrasts, displayed in Figures 6c and 6d,
769 between sub-Saharan regions and the Guinea coast. Notice
770 that there is no signal above the Sahel in high tropospheric
771 levels where moist convection is observed.

772 [52] The east–west circulation has been averaged between
773 15°N and 20°N (Figure 9). Mean values (Figure 9a) point to
774 (1) the summertime Indian east–west cell marked by upward
775 motions over the western part of the Ocean (east of 45°E)
776 and descents over northern Africa (west of 45°E) and (2) the
777 thermal contrast between the cool eastern Atlantic marked
778 by air subsidence and the hot Saharan in the vicinity of the
779 thermal low westward to 5°W marked by atmospheric
780 heating and ascents.

[53] The MED-IND composite (Figure 9b) first shows 781
that ascents in the lower troposphere decrease above the 782
central Sahel, while descents in upper levels are weakened 783
on the eastern Atlantic and above the western (20°W–5°W) 784
and eastern Sahel (15°E–30°E). Then, an area of low-level 785
subsidence anomaly by 30°E–40°E, i.e., associated with the 786
relative Indian cooling, weakens the normal uplifts shown in 787
Figure 9a. Finally, the tropical easterly jet is reinforced by 788
the upper branch of the zonal overturning between the 0° 789
meridian and 20°E. This is in agreement with a reinforce- 790
ment of deep convection processes over central-eastern 791
Sudan-Sahel, since these processes, following *Chen* [2005], 792
are linked to the dynamics of the midtropospheric divergent 793
center maintained by the east–west circulation and the 794
Saharan thermal low. 795

[54] The TNA-TSA composite exhibits few significant 796
upward departures above the northern tropical Atlantic as 797
the thermal response of the atmosphere to the relative sur- 798
face warming. By contrast, no significant signal above 799
Africa (20°W–40°E) can be noticed, except a divergence 800
area at 600 hPa in the Western Sahel and an easterly wind 801
component between 25°E and 45°E in high troposphere. 802

9. Discussion and Conclusion 803

[55] The objective of this study was to revisit the question 804
of the July–September SST–African rainfall teleconnection 805
variability in separating basin-scale variability from the 806
direct impact of the quasi-global thermal evolution observed 807
since 1900, regardless of its natural or anthropogenic origin. 808
Using statistical methods such as linear correlation, linear 809
multiple regression, composite and cluster analyses, the 810
results confirmed that the relationship is rather linear 811
without significant differences between African longitudes 812
but concerns more the Sahelian belt than the subequatorial 813
zone. Interestingly, the SST–Sahel teleconnection appears 814
more often significant with the Mediterranean index (positive 815
correlation) and with the Indian Ocean (negative correlation) 816
all along the period in about 50% of years. By contrast, sig- 817
nificant correlations observed with SSTs in other basins are 818
less frequent: only in the 1950s–1970s, during the negative 819
trend in Sahelian rainfall, for the southern Atlantic basin and 820
the meridional Atlantic dipole; Only during the anomalous 821
1970s–1980s dry period for the western Pacific region and 822
since the end of the 1960s for the Nino area. 823

[56] Analyzing the relationship in a more global context 824
through both regional rainfall estimates and atmospheric 825
indices representative of the African monsoon intensity 826
(WAMI and $-\omega$), we showed that the quasi-global warming 827
(GSST) explains a small part of the relationship except with 828
vertical ascents above the African Sahel. The tropical 829
Atlantic and equatorial Pacific signals impact also moder- 830
ately. Overall, the dominant statistical linkage, both in terms 831
of intensity and time stability, is found with the Mediterra- 832
nean basin and with the Indian Ocean. In the recent period, 833
marked by a moderate rainfall recovery, the teleconnection 834
decreases in the southern tropical Atlantic and Indian Ocean 835
and increases with GSST and over the Mediterranean and 836
Nino areas. 837

[57] Additional regression and cluster analyses allowed us 838
to focus more on the SST signals observed in the oceanic 839
basins close to the African continent. We showed that, with 840

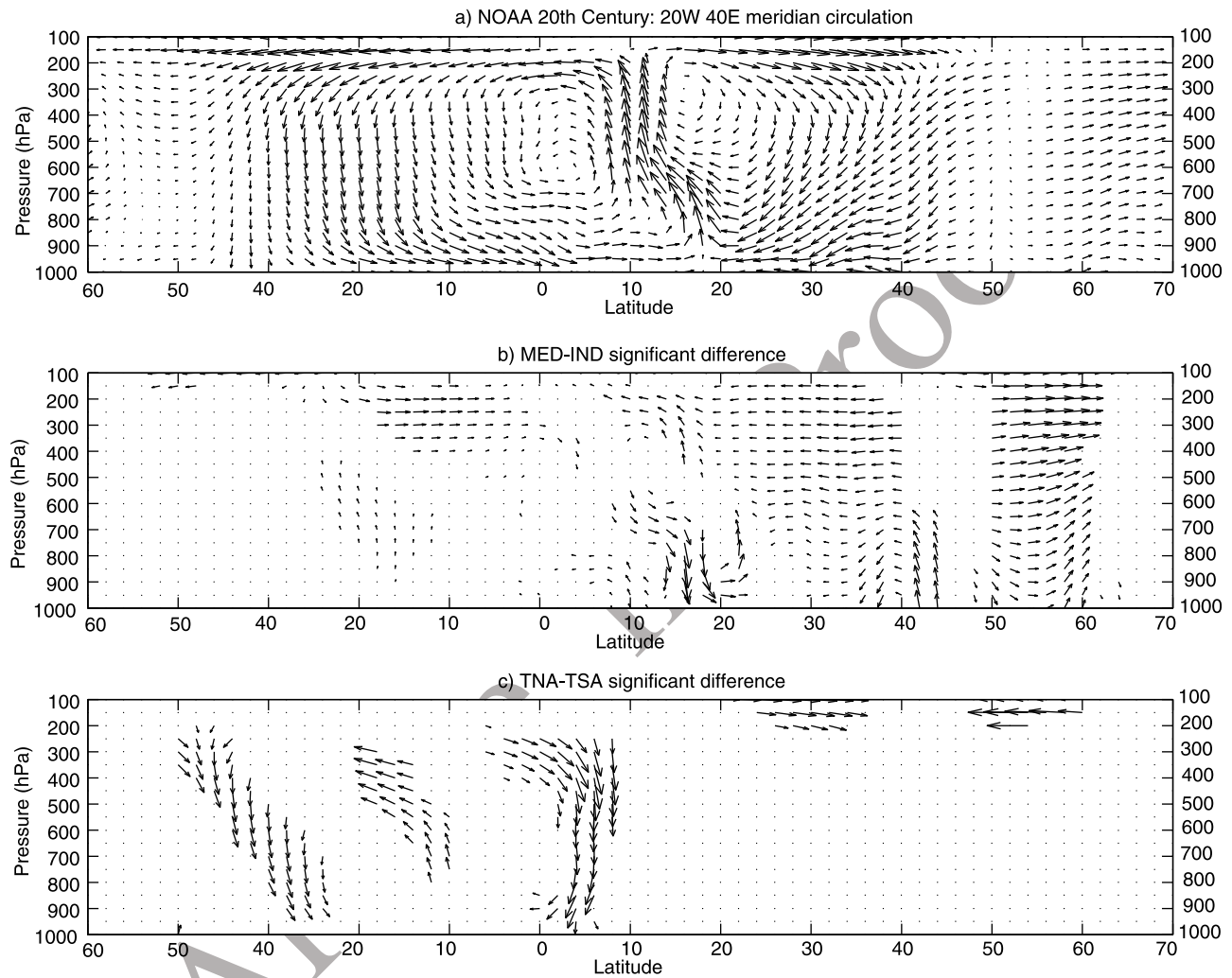


Figure 8. July–September atmospheric circulation (divergent wind, $-\omega$) along a meridional-vertical plane averaged between 20°W and 40°E over the period 1920–2008. (a) Mean values, (b) MED-IND composite relative to SST differences between the eastern Mediterranean basin and the Indian Ocean, and (c) TNA-TSA composite relative to SST differences between the northern and southern tropical Atlantic basins. In Figures 8b and 8c, only the significant values are displayed. The statistical significance has been estimated on the vertical and meridional components through a Student t test contrasting the 20 highest and the 20 lowest seasonal differences versus all the remainders.

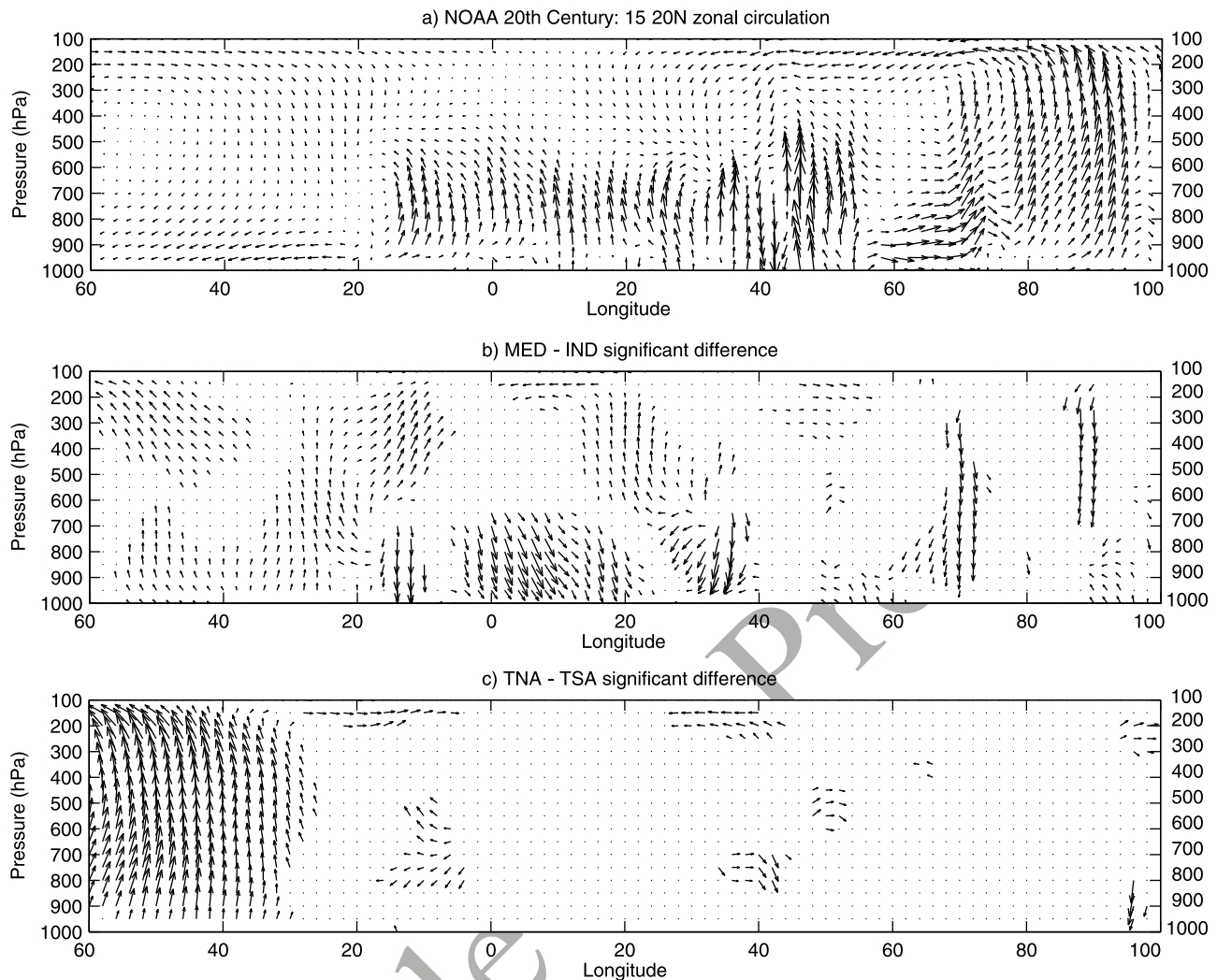


Figure 9. Same as Figure 8 but for the July–September atmospheric circulation along a zonal-vertical plane averaged between 15°N and 20°N.

841 a statistical point of view, the TNA-TSA differences (the
842 Atlantic dipole) are less efficient than the MED-IND dif-
843 ferences to discriminate correctly the Sahelian rainfall
844 anomalies: wetter (drier) rainy seasons are primarily asso-
845 ciated with warmer (colder) anomalies in the Mediterranean,
846 and colder (warmer) anomalies in the Indian Ocean. Indeed
847 more than two thirds of the rainy seasons classified as dry
848 (wet) are concomitant of negative (positive) MED-IND
849 differences; these scores reach 16 out of 18 (12 out of 15)
850 for the rainy seasons classified as very dry (very wet).

851 [58] The connection observed with continental precipita-
852 tion over a larger domain (60°W–60°E) confirmed this
853 feature and showed that removing linear trends in the SST
854 series decreases correlation values without changing dras-
855 tically the spatial patterns. The statistical effects of SST
856 variability on the 950 hPa moisture flux field and over-
857 turning circulation along the meridional and zonal planes
858 have been also depicted. The results obtained can be sum-
859 marized as follows.

860 [59] Positive TNA-TSA differences tend to generate
861 opposite rainfall anomalies along the meridional plane, i.e.,
862 above normal rainfall in sub-Saharan regions and below

normal amounts across the equatorial Atlantic (Guinean 863
coast, north Brazil). A northward SST gradient in the 864
tropical Atlantic is mainly associated with: (1) significant 865
upward atmospheric motion, a thermal response of the 866
atmosphere to the surface warming in the northern basin; 867
(2) a reinforcement of the moisture transport from the 868
southeast over the western equatorial Atlantic and the Sahe- 869
lian belt; and (3) a general subsidence anomaly above 5°N 870
over Africa in the whole troposphere. The two last points are 871
coherent with the dipolar rainfall response over the Sahelian 872
and Guinean regions. 873

[60] By contrast, the positive MED-IND differences are 874
concomitant with rainfall excess over the whole Sudan-Sahel 875
belt and with rainfall drying in Brazil and central Europe. 876
This is associated with an enhancement of both the north- 877
easterly moisture transport from the eastern Mediterranean 878
and the monsoon southwesterly moisture transport from the 879
eastern equatorial Atlantic by the monsoon flow. Such 880
rainfall and atmospheric patterns reproduce well several 881
elements of the teleconnection observed between the Med- 882
iterranean and the African monsoon [Rowell, 2003; Raicich 883
et al., 2003; Fontaine *et al.*, 2009]. However, four additional 884

885 signals have been reported in the monsoon region: (1) a
886 subsidence departure from midlevels above 10°N–18°N
887 associated with air ascents above the Saharan thermal lows;
888 (2) upward anomalies on the western and eastern Sahel
889 reinforcing the normal atmospheric ascents linked to deep
890 convection in upper levels; (3) a low-level subsidence
891 anomaly by 30°E–40°E in agreement with the Indian
892 cooling weakening the normal uplifts; and (4) a rein-
893 forcement of the tropical easterly jet over 0°–20°E.

894 [61] **Acknowledgments.** The authors are grateful to the University of
895 East Anglia, Global Precipitation Climatology Centre (GPCP), the National
896 Oceanic and Atmospheric Administration, the National Center for Atmo-
897 spheric Research, and National Centers for Environmental Prediction for
898 providing most of the data presented in section 2. The study was sup-
899 ported by the TELEMEDAF (Italian CNR/French CNRS joint project) and
900 by the Global Change and Ecosystems program EU Integrated project:
901 African Monsoon Multidisciplinary Analysis (AMMA) and the French
902 component of AMMA. Based on a French initiative, AMMA was built by
903 an international scientific group and has been funded by a large number
904 of agencies, especially from France, U. K., United States, and Africa. It has
905 been the beneficiary of a major financial contribution from the European
906 Community's Sixth Framework Research Programme. Calculations were per-
907 formed using HPC resources from DSI-CCUB (Université de Bourgogne).

908 References

- 909 Annamalai, H., S.-P. Xie, J. P. McCreary, and R. Murtugudde (2005),
910 Impact of Indian Ocean sea surface temperature on developing El Niño,
911 *J. Clim.*, *18*, 302–319, doi:10.1175/JCLI-3268.1.
- 912 Bader, J., and M. Latif (2003), The impact of decadal-scale Indian Ocean
913 sea surface temperature anomalies on Sahelian rainfall and the North
914 Atlantic Oscillation, *Geophys. Res. Lett.*, *30*(22), 2169, doi:10.1029/
915 2003GL018426.
- 916 Bader, J., and M. Latif (2011), The 1983 drought in the West Sahel: A case
917 study, *Clim. Dyn.*, doi:10.1007/s00382-009-0700-y, in press.
- 918 Beck, C., J. Grieser, and B. Rudolf (2005), A new monthly precipitation
919 climatology for the global land areas for the period 1951 to 2000, in
920 *DWD, Klimastatusbericht 2004*, pp. 181–190, German Weather Serv.,
921 Offenbach, Germany.
- 922 Bell, M. A., and P. J. Lamb (2006), Integration of weather system variability
923 to multidecadal regional climate change: The West African Sudan–Sahel
924 zone, 1951–98, *J. Clim.*, *19*, 5343–5365, doi:10.1175/JCLI4020.1.
- 925 Biasutti, M., and A. Giannini (2006), Robust Sahel drying in response to
926 late 20th century forcings, *Geophys. Res. Lett.*, *33*, L11706,
927 doi:10.1029/2006GL026067.
- 928 Biasutti, M., I. M. Held, A. H. Sobel, and A. Giannini (2008), SST forcings
929 and Sahel rainfall variability in simulations of the twentieth and twenty-
930 first centuries, *J. Clim.*, *21*, 3471–3486, doi:10.1175/2007JCLI1896.1.
- 931 Caminada, C., and L. Terray (2010), Twentieth century Sahel rainfall vari-
932 ability as simulated by the ARPEGE AGCM, and future changes, *Clim.*
933 *Dyn.*, *35*, 75–94, doi:10.1007/s00382-009-0545-4.
- 934 Charney, J., W. J. Quirk, S.-H. Chow, and J. Kornfield (1977), A compara-
935 tive study of the effects of albedo change on drought in semi-arid regions,
936 *J. Atmos. Sci.*, *34*, 1366–1385, doi:10.1175/1520-0469(1977)034<1366:
937 ACSOTE>2.0.CO;2.
- 938 Chen, T.-C. (2005), Maintenance of the midtropospheric North African
939 summer circulation: Saharan high and African easterly jet, *J. Clim.*, *18*,
940 2943–2962, doi:10.1175/JCLI3446.1.
- 941 Compo, G. P., J. S. Whitaker, and P. D. Sardeshmukh (2006), Feasibility of
942 a 100 year reanalysis using only surface pressure data, *Bull. Am. Meteorol.*
943 *Soc.*, *87*, 175–190, doi:10.1175/BAMS-87-2-175.
- 944 Delworth, T. L., S. Manabe, and R. J. Stouffer (1993), Interdecadal varia-
945 tions of the thermohaline circulation in a coupled ocean–atmosphere
946 model, *J. Clim.*, *6*, 1993–2011, doi:10.1175/1520-0442(1993)
947 006<1993:IVOTTC>2.0.CO;2.
- 948 Folland, C. K., T. N. Palmer, and D. E. Parmer (1986), Sahel rainfall and
949 worldwide sea temperatures, *Nature*, *320*, 602–607, doi:10.1038/
950 320602a0.
- 951 Fontaine, B., S. Janicot, and V. Moron (1995), Rainfall anomaly patterns
952 and wind field signals over West Africa in August (1958–1989), *J. Clim.*,
953 *8*, 1503–1510, doi:10.1175/1520-0442(1995)008<1503:RAPAWF>2.0.
954 CO;2.
- 955 Fontaine, B., J. Garcia-Serrano, P. Roucou, B. Rodriguez-Fonseca, T. Losada,
956 F. Chauvin, S. Gervois, S. Sivarajan, P. Ruti, S. Janicot (2009), Impacts
of warm and cold situations in the Mediterranean basins on the West
African monsoon: Observed connection patterns (1979–2006) and cli-
mate simulations, *Clim. Dyn.*, *35*, 95–114, doi:10.1007/s00382-009-
0599-3.
- Gaetani, M., B. Fontaine, P. Roucou, and M. Baldi (2010), Influence of the
Mediterranean Sea on the West African Monsoon: Intraseasonal variability
in numerical simulations, *J. Geophys. Res.*, *115*, D24115, doi:10.1029/
2010JD014436.
- Giannini, A., R. Saravanan, and P. Chang (2003), Oceanic forcing of
Sahel rainfall on interannual to interdecadal time scales, *Science*,
302, 1027–1030, doi:10.1126/science.1089357.
- Goldenberg, S. B., et al. (2001), The recent increase in Atlantic hurricane
activity: Causes and implications, *Science*, *293*, 474–479, doi:10.1126/
science.1060040.
- Hastenrath, S., and P. J. Lamb (1977), *Climatic Atlas of the Tropical Atlan-
tic and Eastern Pacific Oceans*, Univ. of Wis. Press, Madison.
- Hastenrath, S., and D. Polzin (2011), Long-term variations of circulation in
the tropical Atlantic sector and Sahel rainfall, *Int. J. Climatol.*,
doi:10.1002/joc.2116, in press.
- Hodson, D. L. R., R. T. Sutton, C. Cassou, N. Keenlyside, Y. Okumura,
and T. Zhou (2010), Climate impacts of recent multidecadal changes in
Atlantic Ocean sea surface temperature: A multimodel comparison, *Clim.*
Dyn., *34*, 1041–1058, doi:10.1007/s00382-009-0571-2.
- Izumo, T., J. Vialard, M. Lengaigne, C. de Boyer Montegut, S.-K. Behera,
J. J. Luo, S. Cravatte, S. Masson, and T. Yamagata (2010), Influence of
the state of the Indian Ocean Dipole on the following year's El Niño, *Nat.*
Geosci., *3*, 168–172, doi:10.1038/ngeo760.
- Janicot, S., S. Trzaska, and I. Poccarrd (2001), Summer Sahel–ENSO tele-
connection and decadal time scale SST variations, *Clim. Dyn.*, *18*,
303–320, doi:10.1007/s003820100172.
- Joly, M., and A. Volodre (2009), Influence of ENSO on the West African
monsoon: Temporal aspects and atmospheric processes, *J. Clim.*, *22*,
3193–3210, doi:10.1175/2008JCLI2450.1.
- Joly, M., and A. Volodre (2010), Role of the Gulf of Guinea in the inter-
annual variability of the West African monsoon: What do we learn from
CMIP3 coupled simulations?, *Int. J. Climatol.*, *30*, 1843–1856,
doi:10.1002/joc.2026.
- Kim, K.-M., W.-K. Lau, Y. C. Sud, and G. K. Walker (2010), Influence of
aerosol-radiative forcings on the diurnal and seasonal cycles of rainfall
over West Africa and eastern Atlantic Ocean using GCM simulations,
Clim. Dyn., *35*, 115–126, doi:10.1007/s00382-010-0750-1.
- Lamb, P. J. (1978), Large-scale tropical Atlantic surface circulation patterns
associated with Subsaharan weather anomalies, *Tellus*, *30*, 240–251,
doi:10.1111/j.2153-3490.1978.tb00839.x.
- Losada, T., B. Rodriguez-Fonseca, S. Janicot, S. Gervois, F. Chauvin, and
P. Ruti (2009), Tropical response to the Atlantic equatorial mode: impact
on the West African monsoon, *Clim. Dyn.*, *35*, 29–43, doi:10.1007/
s00382-009-0625-5.
- Lough, J. M. (1986), Tropical Atlantic sea surface temperature and rainfall
variations in subsaharan Africa month, *Mon. Weather Rev.*, *114*, 561–570,
doi:10.1175/1520-0493(1986)114<0561:TASSTA>2.0.CO;2.
- Mitchell, T. D., T. R. Carter, P. D. Jones, M. Hulme, and M. New (2004),
A comprehensive set of high-resolution grids of monthly climate for
Europe and the globe: The observed record (1901–2000) and 16 scenarios
(2001–2100), *Tyndall Working Pap.* 55, Tyndall Cent., UEA, Norwich,
U. K. (Available at <http://www.tyndall.ac.uk/>)
- Mohino, E., S. Janicot, and J. Bader (2011), Sahelian rainfall and
decadal to multidecadal SST variability, *Clim. Dyn.*, doi:10.1007/
s00382-010-0867-2, in press.
- Murakami, M. (1979), Large scale aspects of deep convective activity over
the Gate area, *Mon. Weather Rev.*, *107*, 994–1013, doi:10.1175/1520-
0493(1979)107<0994:LSAODC>2.0.CO;2.
- New, M., D. Lister, M. Hulme, and I. Makin (2002), A high-resolution data
set of surface climate over global land areas, *Clim. Res.*, *21*, 1–25,
doi:10.3354/cr021001.
- Nicholson, S. E. (1979), Revised rainfall series for the West African sub-
tropics, *Mon. Weather Rev.*, *107*, 620–623, doi:10.1175/1520-0493
(1979)107<0620:RRSFTW>2.0.CO;2.
- Nicholson, S. E., and R. S. Nyenzi (1990), Temporal and spatial variability
of SSTs in tropical Atlantic and Indian oceans, *Meteorol. Atmos. Phys.*,
42, 1–17, doi:10.1007/BF01030575.
- Paeth, H., and A. Hense (2004), SST versus climate change signals in West
African rainfall: 20th century variations and future projections, *Clim.*
Change, *65*, 179–208, doi:10.1023/B:CLIM.0000037508.88115.8a.
- Palmer, T. N. (1986), The influence of the Atlantic, Pacific and Indian
oceans on Sahel rainfall, *Nature*, *322*, 251–253, doi:10.1038/322251a0.
- Polo, I., B. Rodriguez-Fonseca, T. Losada, and J. Garcia-Serrano (2008),
Tropical Atlantic variability modes (1979–2002). Part I: Time-evolving

- 1035 SST modes related to West African rainfall, *J. Clim.*, *21*, 6457–6475, 1065
 1036 doi:10.1175/2008JCLI2607.1. 1066
- 1037 Polyakov, I. V., V. A. Alexeev, U. S. Bhatt, E. I. Polyakova, and X. Zhang 1067
 1038 (2010), North Atlantic warming: Patterns of long-term trend and multi- 1068
 1039 decadal variability, *Clim. Dyn.*, *34*, 439–457, doi:10.1007/s00382-008- 1069
 1040 0522-3. 1070
- 1041 Raicich, F., N. Pinardi, and A. Navarra (2003), Teleconnections between 1071
 1042 Indian monsoon and Sahel rainfall and the Mediterranean, *Int. J. Climatol.*, 1072
 1043 *23*, 173–186, doi:10.1002/joc.862. 1073
- 1044 Rodríguez de Fonseca, B., et al. (2011), Interannual and decadal SST 1074
 1045 forced responses of the West African monsoon, *Atmos. Sci. Lett.*, in 1075
 1046 press. 1076
- 1047 Rodríguez-Fonseca, B., I. Polo, J. García-Serrano, T. Losada, E. Mohino, 1077
 1048 C. R. Mechoso, and F. Kucharski (2009), Are Atlantic Niños enhancing 1078
 1049 Pacific ENSO events in recent decades?, *Geophys. Res. Lett.*, *36*, 1079
 1050 L20705, doi:10.1029/2009GL040048. 1080
- 1051 Rowell, D. P. (2003), The impact of Mediterranean SSTs on the Sahelian 1081
 1052 rainfall season, *J. Clim.*, *16*, 849–862, doi:10.1175/1520-0442(2003) 1082
 1053 016<0849:TIOMSO>2.0.CO;2. 1083
- 1054 Rowell, D. P., C. K. Folland, K. Maskell, and M. N. Ward (1995), Variabil- 1084
 1055 ity of summer rainfall over tropical north Africa (1906–92): Observations 1085
 1056 and modelling, *Q. J. R. Meteorol. Soc.*, *121*, 669–704. 1086
- 1057 Saha, S., et al. (2006), The NCEP Climate Forecast System, *J. Clim.*, *19*, 1087
 1058 3483–3517, doi:10.1175/JCLI3812.1. 1088
- 1059 Smith, T. M., R. W. Reynolds, T. C. Peterson, and J. Lawrimore (2008), 1089
 1060 Improvements to NOAA's historical merged land-ocean surface temper- 1090
 1061 ature analysis (1880–2006), *J. Clim.*, *21*, 2283–2296. doi:10.1175/ 1091
 1062 2007JCLI2100.1. 1092
- 1063 Stott, P. A., S. F. B. Tett, G. S. Jones, M. R. Allen, J. F. B. Mitchell, and G. J. 1093
 1064 Jenkins (2000), External control of 20th century temperature by natural 1094
 and anthropogenic forcings, *Science*, *290*, 2133–2136, doi:10.1126/ 1095
 science.290.5499.2133. 1096
- Walker, J., and P. R. Rowntree (1977), The effect of soil moisture on circula- 1097
 tion and rainfall in a tropical model, *Q. J. R. Meteorol. Soc.*, *103*, 29–46, 1098
 doi:10.1002/qj.49710343503. 1099
- Ward, M. N. (1998), Diagnosis and short-lead time prediction of summer 1100
 rainfall in tropical North Africa at interannual and multidecadal time- 1101
 scales, *J. Clim.*, *11*, 3167–3191, doi:10.1175/1520-0442(1998) 1102
 011<3167:DASLTP>2.0.CO;2. 1103
- Ward, M. N., C. K. Folland, K. Maskell, D. Rowell, and A. Colman (1990), 1104
 Understanding and predicting seasonal rainfall in subSaharan Africa, 1105
Trop. Meteorol. Res. Programme Rep. Ser. 36, pp. 157–161, WMO, 1106
 Geneva, Switzerland. 1107
- Xue, Y., R. W. A. Hutjes, R. J. Harding, M. Claussen, S. Prince, E. F. 1108
 Lambin, S. J. Allen, P. Dirmeyer, and T. Oki (2004), The Sahelian climate, 1109
 in *Vegetation, Water, Humans and the Climate*, edited by P. Kabat et al., 1110
 pp. 59–77, Springer, Berlin. 1111
- Zeng, N., J. D. Neelin, K. M. Lau, and C. J. Tucker (1999), Enhancements 1112
 of interdecadal climate variability in the Sahel by vegetation interaction, 1113
Science, *286*, 1537–1540, doi:10.1126/science.286.5444.1537. 1114
- Zhang, R., and T. L. Delworth (2006), Impact of Atlantic multidecadal oscil- 1115
 lations on India/Sahel rainfall and Atlantic hurricanes, *Geophys. Res. Lett.*, 1116
33, L17712, doi:10.1029/2006GL026267. 1117
- B. Fontaine, P. Roucou, and A. Ullmann, Centre de Recherches de 1118
 Climatologie, CNRS/Université de Bourgogne, 6 Boulevard Gabriel, F- 1119
 21000 Dijon, France. (fontaine@u-bourgogne.fr) 1120
 M. Gaetani, Istituto di Biometeorologia, IBIMET-CNR, Via dei Taurini 1121
 19, I-00185 Rome, Italy. 1122